



OPEN

Parallel Photonic Quantum Computation Assisted by Quantum Dots in One-Side Optical Microcavities

SUBJECT AREAS:
INFORMATION THEORY
AND COMPUTATION
QUANTUM OPTICSMing-Xing Luo^{1,2,3} & Xiaojun Wang⁴Received
20 February 2014Accepted
30 June 2014Published
17 July 2014Correspondence and
requests for materials
should be addressed to
M.-X.L. (mxluo@home.
swjtu.edu.cn)

¹Information Security and National Computing Grid Laboratory, Southwest Jiaotong University, Chengdu 610031, China, ²State Key Laboratory of Networking and Switching Technology, Beijing University of Posts and Telecommunications, Beijing 100876, China, ³State Key Laboratory of Information Security (Graduate University of Chinese Academy of Sciences), Beijing 100049, China, ⁴School of Electronic Engineering, Dublin City University, Dublin 9, Ireland.

Universal quantum logic gates are important elements for a quantum computer. In contrast to previous constructions on one degree of freedom (DOF) of quantum systems, we investigate the possibility of parallel quantum computations dependent on two DOFs of photon systems. We construct deterministic hyper-controlled-not (hyper-CNOT) gates operating on the spatial-mode and the polarization DOFs of two-photon or one-photon systems by exploring the giant optical circular birefringence induced by quantum-dot spins in one-sided optical microcavities. These hyper-CNOT gates show that the quantum states of two DOFs can be viewed as independent qubits without requiring auxiliary DOFs in theory. This result can reduce the quantum resources by half for quantum applications with large qubit systems, such as the quantum Shor algorithm.

Quantum information processing is very powerful for managing or transmitting information, as the quantum computation^{1–4} and quantum communication^{5–7}. Quantum logic gates or quantum controlled gates^{8,9} are key elements for quantum applications based on the quantum circuit model¹⁰. These gates, especially the controlled-not (CNOT) gate or the controlled phase-flip (CPF) gate, may be implemented using various quantum systems, such as the ion trap¹¹, free electron¹², cavity quantum electrodynamics (QED) system^{13,14}, nuclear magnetic resonance^{15,16}, and quantum dot¹⁷. In 2001, Knill, Laflamme, and Milburn¹⁸ showed that the CNOT gate can be realized with the maximal success probability of 3/4 using linear optical elements and the polarization states of single photons. This scheme has been improved for a near-deterministic CNOT gate using the weak cross-Kerr nonlinearity and the quantum nondemolition measurement¹⁹, which is also used for the unambiguous experimental demonstration of the CNOT operation²⁰. However, a giant Kerr nonlinearity is still a challenge^{21,22} because the initial phase shift achieved at the single-photon level is very small. QED may be a candidate for large nonlinear phase shifts^{23–26}.

Recently, the solid-state quantum system based on an electron spin in a quantum dot (QD) inside a microcavity has attracted much attention because of its optical property and scalability. Hu et al.^{27,28} construct the quantum nondemolition measurement using the giant optical circular birefringence of the one-sided QD-cavity system. The double-sided QD-cavity system can be used to construct an entanglement beam splitter (EBS)²⁹. These systems are also useful for entanglement generation and Bell-state analysis^{27–30}, quantum gates implementation^{31–37}, and hyper-entangled Bell-state analysis^{38,39}. These implementations of the CNOT gate are focused on the same DOF of photon states and have not shown the independence of different DOFs.

In this paper, we consider the CNOT gate on two DOFs of photon states using the optical circular birefringence of a one-sided QD-cavity system. Most previous results are related to the CNOT gate on one DOF of quantum systems, such as the polarization DOF of photon systems or the spin DOF of electron systems. Generally, one DOF [spatial-mode DOF] is used to assist the quantum logic gates on another DOF [polarization DOF]^{18–20}. We investigate the possibility of parallel quantum computation based on two DOFs of photon systems, without using auxiliary spatial modes or polarization modes. We construct six deterministic hyper-controlled-not (hyper-CNOT) gates operating on the spatial-mode and the polarization DOFs of a two-photon or one-photon system, which are beyond the hyper-CNOT gates on the same DOF of two-photon state^{33–35}, hybrid hyper-CNOT gates on the photon and stationary electron spins in quantum dots^{32,36}, or hyper-CNOT gates on two photons³⁷. Our theoretical results show that two DOFs of photon systems can be used as independent qubits in quantum



information processing. With these realizations, one half of the quantum resources may be saved. This saving is very important for quantum applications with large qubit systems, such as the quantum Shor algorithm and quantum communications.

Results

The spatial-mode and the polarization DOFs of a photon can be manipulated easily using linear optical elements^{19,20,31–33}. Thus, it is convenient to use these DOFs as independent qubits in quantum applications. To show the independence of two DOFs of the polarization DOF and spatial DOF of each photon for any quantum schemes, it is necessary to show that all quantum transformations in $SU(2^n)$ may be realized on the two DOFs. Note that the CNOT gate on two qubit states and rotation operations on one qubit are universal quantum logic gates^{8–10} to simulate any quantum transformation in $SU(2^n)$. We only need to realize the CNOT gate on two DOFs of the photon system, while rotation operations on one DOF are easily implemented. Because of the different roles played by each DOF of the photon in a CNOT gate, there are six different forms of one CNOT gate on two DOFs of the photon system, i.e., four CNOT gates on a two-photon system (each DOF of one photon is used) and two CNOT gates on a one-photon system. None of these gates require changing these DOFs during the transformations, nor do they require any auxiliary DOFs. Thus one DOF of one photon may be regarded as the controlling qubit while the other is the goal qubit. Note that the CNOT gate on a two-qubit system and the rotation operations on one-qubit system are universal logic gates for general quantum computation. From our six CNOT gates, all quantum global transformations on the same DOF of multiple photon systems can be realized on different DOFs of these photon systems. In this case, each DOF of the photon systems can be viewed as an independent qubit in quantum applications, which means that one half of quantum resources may be saved.

Quantum-dot-cavity system. To complete our CNOT operations, the following optical property^{40–46} and QD-cavity system are used for our schemes. The QD-cavity system used in our proposal is constructed by a singly charged QD [a self-assembled In(Ga)As QD or a GaAs interface QD] located in the center of a one-sided optical resonant cavity to achieve the maximal light-matter coupling, as shown in Figure 1. According to the Pauli exclusion principle⁴⁵, a negatively charged exciton X^- consisting of two electrons bound to one hole can be optically excited when an excess electron is injected into QD. For the excess electron-spin state $|\uparrow\rangle$ or $|\downarrow\rangle$, a negatively charged exciton $|\uparrow\downarrow\rangle$ or $|\downarrow\uparrow\rangle$ with two electron spins antiparallel⁴⁶ is created by resonantly absorbing $|L\rangle$ [left circularly polarized photon] or $|R\rangle$ [right circularly polarized photon], respectively.

Here, $|\uparrow\rangle$ and $|\downarrow\rangle$ describe the heavy-hole spin states $\left|+\frac{3}{2}\right\rangle$ and $\left|-\frac{3}{2}\right\rangle$, respectively.

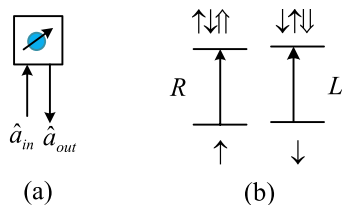


Figure 1 | Schematic X^- spin-dependent transitions with circularly polarized photons. (a) A charged QD inside a one-side micropillar microcavity interacting with circularly polarized photons. \hat{a}_{in} and \hat{a}_{out} are the input and output field operators of the waveguide, respectively. (b) X^- spin-dependent optical transition rules due to the Pauli exclusion principle. $|L\rangle$ and $|R\rangle$ represent the left and right circularly polarized photon, respectively. $|\uparrow\rangle$ and $|\downarrow\rangle$ represent the spins of the excess electron.

The input-output relation of this single-sided QD-cavity system can be calculated from the Heisenberg equations⁴⁶ of motions for the cavity field operator \hat{a} and dipole operator σ_- ,

$$\begin{cases} \frac{d\hat{a}}{dt} = -(i\Delta\omega_c + \eta + \kappa_s)\hat{a} - g\hat{\sigma}_- - \sqrt{\eta}\hat{a}_{in}, \\ \frac{d\hat{\sigma}_-}{dt} = -(i\Delta\omega_e + \zeta)\hat{\sigma}_- - g\hat{\sigma}_z\hat{a}, \end{cases} \quad (1)$$

where $\Delta\omega_c = \omega_c - \omega$, $\Delta\omega_e = \omega_e - \omega$, ω_c , ω_e and ω are the frequencies of the cavity mode, the input probe light, and the X^- transition, respectively. g is the coupling strength between the cavity and X^- . ζ , η , and κ_s are the decay rates of the X^- , the cavity field, and the cavity side leakage mode, respectively. \hat{a}_{in} and \hat{a}_{out} satisfy $\hat{a}_{out} = \hat{a}_{in} + \sqrt{\kappa}\hat{a}$. If X^- stays in the ground state most of the time²⁷ [$\langle\sigma_z\rangle = -1$], the reflection coefficient of the QD-cavity system is

$$r(\omega) = \frac{i\Delta\omega_c - \kappa_s + \kappa + \hat{g}}{i\Delta\omega_c + \kappa_s + \kappa + \hat{g}}, \quad (2)$$

where $\hat{g} = g^2/(i\Delta\omega_e + \zeta)$. Considering the coupling strength $g = 0$, the QD is uncoupled from the cavity (the cold cavity), and the reflection coefficient in equation (2) becomes

$$r_0(\omega) = \frac{i\Delta\omega_c - \kappa_s + \kappa}{i\Delta\omega_c + \kappa_s + \kappa}. \quad (3)$$

Thus, the optical process based on the X^- spin-dependent transitions is obtained^{27,34}. For a light in the state $|L\rangle$, a phase shift θ_h is followed for the hot cavity (the QD is coupled from the cavity) with the excess electron spin $|\uparrow\rangle$, or a phase shift θ_0 is followed for the cold cavity with the excess electron spin $|\downarrow\rangle$. For a light in the state $|R\rangle$, the phase shift θ_0 is followed for the cold cavity with the excess electron spin $|\uparrow\rangle$, and the phase shift θ_h is gotten for the hot cavity with the excess electron spin $|\downarrow\rangle$. By adjusting the frequencies of the light (ω) and the cavity mode (ω_c), the reflection coefficients can reach $|r_0(\omega)| \approx 1$ and $|r_h(\omega)| \approx 1$ when the cavity side leakage is negligible. If the linearly polarized probe beam in the state $\alpha|R\rangle + \beta|L\rangle$ is put into a one-sided QD-cavity system in the superposition spin state $(|\uparrow\rangle + |\downarrow\rangle)/\sqrt{2}$, the state of the system consisting of the light and the electron spin after reflection is

$$|\uparrow\rangle(\alpha e^{i\theta_0}|R\rangle + \beta e^{i\theta_h}|L\rangle) + |\downarrow\rangle(\alpha e^{i\theta_h}|R\rangle + \beta e^{i\theta_0}|L\rangle), \quad (4)$$

where $\theta_0 = \arg[r_0(\omega)]$ and $\theta_h = \arg[r_h(\omega)]$. By adjusting the frequencies ω and ω_c , one can get the phase shifts of the left and the right circularly polarized photons as $\theta_0 = \pi$ and $\theta_h = 0$. From equation (4), the interaction of a single photon with a QD-cavity system can be described as²⁷

$$\begin{aligned} |R\rangle|\uparrow\rangle &\mapsto -|R\rangle|\uparrow\rangle, |R\rangle|\downarrow\rangle \mapsto |R\rangle|\downarrow\rangle, \\ |L\rangle|\uparrow\rangle &\mapsto |L\rangle|\uparrow\rangle, |L\rangle|\downarrow\rangle \mapsto -|L\rangle|\downarrow\rangle. \end{aligned} \quad (5)$$

Spatial-CNOT gate on a two-photon system. The schematic deterministic CNOT gates on the same DOF of a two-photon system are shown in Figure 2. Here, the circuit shown in Figure 2(a) is designed for the deterministic CNOT gate on the spatial modes of two photons using a one-sided QD-cavity system. The spatial-mode state of the photon a is the control qubit, while the spatial-mode state of the photon b is the target qubit. The initial state of the excess electron spin e in QD is $|+\rangle_e = 1/\sqrt{2}(|\uparrow\rangle + |\downarrow\rangle)_e$. The initial state of the photon a is $|\phi\rangle_a = (\alpha_1|R\rangle + \alpha_2|L\rangle)_a \otimes (\gamma_1|a_1\rangle + \gamma_2|a_2\rangle)$, where $|a_1\rangle$ and $|a_2\rangle$ represent two spatial modes of the photon a . The detailed circuit is described as follows.

First, the photon a from the spatial mode a_2 passes through the subcircuit S1 [CPBS, X, QD, X, CPBS, sequentially]. From the equation (4), the joint system of the excess electron spin e and the photon

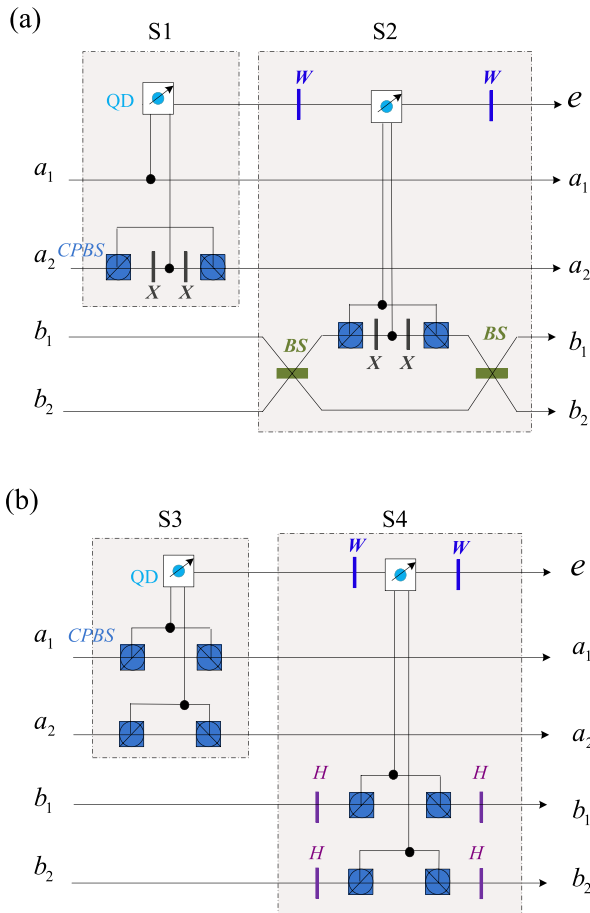


Figure 2 | Schematic hyper-CNOT gate on a two-photon system. (a) Schematic spatial-CNOT gate operating on the spatial-mode degrees of freedom of a two-photon system simultaneously. CPBS represents a polarizing beam splitter in the circular basis, which transmits $|R\rangle$ and reflects $|L\rangle$. BS represents a 50%50 beam splitter to perform the Hadamard operation on the spatial-mode DOF of a photon. X represents the bit-flip operation $X = |R\rangle\langle L| + |L\rangle\langle R|$. W represents the Hadamard operation on the excess electron spin e in QD. (b) Schematic polarization-CNOT gate operating on the polarization degrees of freedom of a two-photon system simultaneously. H represents a half-wave plate (HWP) to perform the Hadamard operation on the polarization DOF of a photon. S1, S2, S3, S4 denote four subcircuits.

a is changed from $|\Phi_0\rangle_{ae} = |\phi\rangle_a \otimes |+\rangle_e$ to

$$|\Phi_1\rangle_{ae} = \frac{1}{\sqrt{2}} [|\uparrow\rangle_e(\gamma_1|a_1\rangle + \gamma_2|a_2\rangle) + |\downarrow\rangle_e(\gamma_1|a_1\rangle - \gamma_2|a_2\rangle)] \otimes (\alpha_1|R\rangle + \alpha_2|L\rangle). \quad (6)$$

This is the controlled-Z gate (CZ_{es}) on the electron spin e and the spatial-mode state of the photon a [with the electron spin e as the control qubit and the photon a as the target qubit], i.e.,

$$CZ_{es} := |\uparrow\rangle_e\langle\uparrow|(|a_1\rangle\langle a_1| + |a_2\rangle\langle a_2|) + |\downarrow\rangle_e\langle\downarrow|(|a_2\rangle\langle a_1| + |a_1\rangle\langle a_2|). \quad (7)$$

Then, the photon b with the form $|\psi\rangle_b = (\beta_1|R\rangle + \beta_2|L\rangle) \otimes (\delta_1|b_1\rangle + \delta_2|b_2\rangle)$ passes a BS (the spatial Hadamard transformation) in the subcircuit S2 and is changed into $|\psi'\rangle_b = (\beta_1|R\rangle + \beta_2|L\rangle) \otimes (\delta'_1|b_1\rangle + \delta'_2|b_2\rangle)$ with $\delta'_1 = (\delta_1 + \delta_2)/\sqrt{2}$ and $\delta'_2 = (\delta_1 - \delta_2)/\sqrt{2}$. At the same time, the joint system of the electron spin e and the photon a is changed from $|\Phi_1\rangle_{ae}$ to

$$|\Phi'_1\rangle_{ae} = (\gamma_1|\uparrow\rangle_e|a_1\rangle + \gamma_2|\downarrow\rangle_e|a_2\rangle) \otimes (\alpha_1|R\rangle + \alpha_2|L\rangle) \quad (8)$$

after one W operation being performed on the electron spin e .

Third, the photon b passes the CPBS, X, QD, X, CPBS, sequentially [subcircuit S2], i.e., another controlled-Z gate shown in equation (7) is performed on the electron spin e and the spatial-mode state of the photon b . The joint system of the electron spin e and the photons a and b is changed from $|\Phi'_1\rangle_{ae} \otimes |\psi'\rangle_b$ to

$$|\Phi''_1\rangle_{eab} = [\gamma_1|\uparrow\rangle_e|a_1\rangle(\delta'_1|b_1\rangle + \delta'_2|b_2\rangle) + \gamma_2|\downarrow\rangle_e|a_2\rangle(\delta'_1|b_1\rangle - \delta'_2|b_2\rangle)] \otimes (\alpha_1|R\rangle + \alpha_2|L\rangle) \otimes (\beta_1|R\rangle + \beta_2|L\rangle). \quad (9)$$

Now, by performing the second Hadamard operation W on the electron spin e and the second Hadamard operation (BS) on the spatial-mode DOF of the photon b , $|\Phi''_1\rangle_{eab}$ is changed into

$$|\Phi_2\rangle_{abe} = (\alpha_1|R\rangle + \alpha_2|L\rangle)_a \otimes (\beta_1|R\rangle + \beta_2|L\rangle)_b \otimes \{|\uparrow\rangle_e[\gamma_1|a_1\rangle(\delta_1|b_1\rangle + \delta_2|b_2\rangle) + \gamma_2|a_2\rangle(\delta_2|b_1\rangle + \delta_1|b_2\rangle)] + |\downarrow\rangle_e[\gamma_1|a_1\rangle(\delta_1|b_1\rangle + \delta_2|b_2\rangle) - \gamma_2|a_2\rangle(\delta_2|b_1\rangle + \delta_1|b_2\rangle)]\}. \quad (10)$$

Finally, after measuring the excess electron spin e under the basis $\{|\uparrow\rangle, |\downarrow\rangle\}$, the joint system of the photons a and b collapses into

$$|\Psi_1\rangle_{ab} = (\alpha_1|R\rangle + \alpha_2|L\rangle)_a \otimes (\beta_1|R\rangle + \beta_2|L\rangle)_b \otimes [\gamma_1|a_1\rangle(\delta_1|b_1\rangle + \delta_2|b_2\rangle) + \gamma_2|a_2\rangle(\delta_2|b_1\rangle + \delta_1|b_2\rangle)]. \quad (11)$$

by performing the phase-flip operation $Z = |a_1\rangle\langle a_1| - |a_2\rangle\langle a_2|$ on the spatial mode of the photon a for the measurement outcome $|\downarrow\rangle$ of the excess electron spin e . Thus, the deterministic spatial-CNOT gate is completed.

Polarization-CNOT gate on a two-photon system. The schematic deterministic CNOT gate on the polarization DOFs of a two-photon system is shown in Figure 2(b). Here, the polarization state of the photon a is the control qubit, while the polarization state of the photon b is the target qubit. The initial states of the excess electron spin e and the photons a and b are $|+\rangle_e$, $|\phi\rangle_a$ and $|\psi\rangle_b$, respectively, shown in Figure 2(a). In contrast to the step one of the spatial-CNOT gate shown in Figure 2(a), photon a first passes through the subcircuit S3 [CPBS, QD, CPBS, sequentially]. The joint system of the photon a and the electron spin e is changed from $|\Phi_0\rangle_{ae} = |\phi\rangle_a|+\rangle_e$ to

$$|\Phi_3\rangle_{ae} = \frac{1}{\sqrt{2}} [|\uparrow\rangle_e(\alpha_1|R\rangle + \alpha_2|L\rangle) + |\downarrow\rangle_e(\alpha_1|R\rangle - \alpha_2|L\rangle)] \otimes (\gamma_1|a_1\rangle + \gamma_2|a_2\rangle). \quad (12)$$

This is the controlled-Z gate (CZ_{ep}) on the electron spin e and the polarization DOF of the photon a [with the electron spin e as the control qubit and the photon a as the target qubit], i.e.,

$$CZ_{ep} := |\uparrow\rangle_e\langle\uparrow|(|R\rangle\langle R| + |L\rangle\langle L|) + |\downarrow\rangle_e\langle\downarrow|(|L\rangle\langle R| + |R\rangle\langle L|). \quad (13)$$

Then, by passing two polarization Hadamard operations H in the subcircuit S4, photon b is changed into $|\psi''\rangle_b = (\beta'_1|R\rangle + \beta'_2|L\rangle) \otimes (\delta_1|b_1\rangle + \delta_2|b_2\rangle)$ with $\beta'_1 = (\beta_1 + \beta_2)/\sqrt{2}$ and $\beta'_2 =$

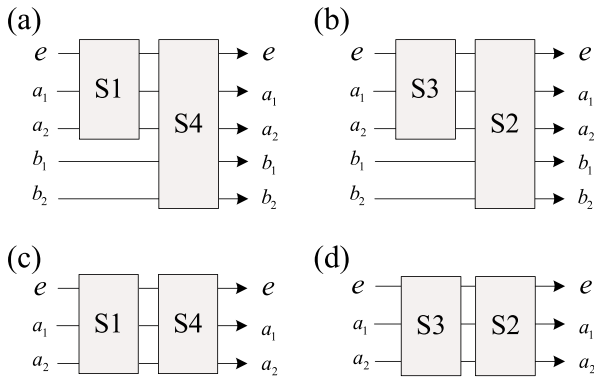


Figure 3 | Schematic hybrid hyper-CNOT gate. (a) Schematic hybrid spatial-polarization CNOT gate on a two-photon system, where a_i and b_i are spatial modes of the photons a and b , respectively. e denotes the excess electron spin in QD. (b) Schematic hybrid polarization-spatial CNOT gate on a two-photon system. (c) Schematic hybrid polarization-spatial CNOT gate on a one-photon system. (d) Schematic hybrid spatial-polarization CNOT gate on a one-photon system. The initial states of photons a and b are $|\phi\rangle_a$ and $|\psi\rangle_b$, respectively. The initial state of the excess electron spin e is $|\uparrow\rangle_e$. S1 and S3 are the two controlled-phase-flip gates described in equations (7) and (13), respectively, shown in Figure 2. S2 and S4 are two controlled-phase-flip gates combined with certain Hadamard operations, shown in Figure 2.

$(\beta_1 - \beta_2)/\sqrt{2}$. The joint system of the photon a and the excess electron spin e may be changed into

$$|\Phi_3\rangle_{ae} = (\alpha_1|\uparrow\rangle_e|R\rangle + \alpha_2|\downarrow\rangle_e|L\rangle) \otimes (\gamma_1|a_1\rangle + \gamma_2|a_2\rangle) \quad (14)$$

by performing one Hadamard operation on the excess electron spin e .

Now, photon b passes through the subcircuit S4 [CPBS, QD, CPBS, sequentially, i.e., another CZ_{ep} operation on the electron spin e and photon b]. The joint system of the excess electron spin e and the photons a and b is changed from $|\Phi_3\rangle_{ae} \otimes |\psi\rangle_b$ to

$$|\Phi_4\rangle_{abe} = [\alpha_1|\uparrow\rangle_e|R\rangle_a(\beta'_1|R\rangle + \beta'_2|L\rangle)_b + \alpha_2|\downarrow\rangle_e|L\rangle_a(\beta'_1|R\rangle - \beta'_2|L\rangle)_b] \otimes (\gamma_1|a_1\rangle + \gamma_2|a_2\rangle) \otimes (\delta_1|b_1\rangle + \delta_2|b_2\rangle). \quad (15)$$

This state may be changed to the following joint system

$$|\Phi_5\rangle_{abe} = \{|\uparrow\rangle_e[\alpha_1|R\rangle_a(\beta|R\rangle + \beta_2|L\rangle)_b + \alpha_2|L\rangle_a(\beta_2|R\rangle + \beta_1|L\rangle)_b] + |\downarrow\rangle_e[\alpha_1|R\rangle_a(\beta_1|R\rangle + \beta_2|L\rangle)_b - \alpha_2|L\rangle_a(\beta_2|R\rangle + \beta_1|L\rangle)_b]\} \otimes (\gamma_1|a_1\rangle + \gamma_2|a_2\rangle) \otimes (\delta_1|b_1\rangle + \delta_2|b_2\rangle) \quad (16)$$

by performing a Hadamard transformation W on the excess electron spin e and performing two Hadamard transformations H on photon b .

Thus, after measuring the electron spin e under the orthogonal basis $\{|\uparrow\rangle, |\downarrow\rangle\}$, photons a and b may be changed into

$$|\Psi_2\rangle_{ab} = [\alpha_1|R\rangle_a(\beta_1|R\rangle + \beta_2|L\rangle)_b + \alpha_2|L\rangle_a(\beta_2|R\rangle + \beta_1|L\rangle)_b] \otimes (\gamma_1|a_1\rangle + \gamma_2|a_2\rangle) \otimes (\delta_1|b_1\rangle + \delta_2|b_2\rangle) \quad (17)$$

by performing the phase-flip transformation $R = |R\rangle\langle R| - |L\rangle\langle L|$ on the polarization of the photon a for the measurement outcome $|\downarrow\rangle$ of

the excess electron spin e . Thus the deterministic polarization-CNOT gate on two photons is completed.

Hybrid spatial-polarization CNOT gate on a two-photon system.

The schematic deterministic hybrid spatial-polarization CNOT gate on the two-photon system is shown in Figure 3(a). Here, the spatial state of photon a is the control qubit, while the polarization state of the photon b is the target qubit. All initial states are identical to ones for the spatial-CNOT gate on the two-photon system shown in Figure 2. The new circuit is derived from both subcircuits in Figure 2. Firstly, the subcircuit S1 shown in Figure 2(a) is used to complete the controlled-phase-flip gate described in equation (7) on the electron spin e and photon a , following the joint system $|\Phi_3\rangle_{ae}$ shown in equation (12). Then, using the subcircuit S4 shown in Figure 2(b) for the excess electron spin e and photon b , the total system is changed from $|\Phi_1\rangle_{ae}|\psi\rangle_b$ to

$$|\Phi_5\rangle_{abe} = \{|\uparrow\rangle_e[\gamma_1|a_1\rangle(\beta_1|R\rangle + \beta_2|L\rangle)_b + \gamma_2|a_2\rangle(\beta_2|R\rangle + \beta_1|L\rangle)_b] + |\downarrow\rangle_e[\gamma_1|a_1\rangle(\beta_1|R\rangle + \beta_2|L\rangle)_b - \gamma_2|a_2\rangle(\beta_2|R\rangle + \beta_1|L\rangle)_b]\} \otimes (\alpha_1|R\rangle + \alpha_2|L\rangle)_a \otimes (\delta_1|b_1\rangle + \delta_2|b_2\rangle)_b. \quad (18)$$

Thus, after measuring the excess electron spin e under the orthogonal basis $\{|\uparrow\rangle, |\downarrow\rangle\}$, the photons a and b may be transformed as follows:

$$|\Psi_3\rangle_{ab} = [\gamma_1|a_1\rangle(\beta_1|R\rangle + \beta_2|L\rangle)_b + \gamma_2|a_2\rangle(\beta_2|R\rangle + \beta_1|L\rangle)_b] \otimes (\alpha_1|R\rangle + \alpha_2|L\rangle)_a \otimes (\delta_1|b_1\rangle + \delta_2|b_2\rangle) \quad (19)$$

by performing the phase-flip operation Z on the spatial DOFs of the photon a for the measurement outcome $|\downarrow\rangle$ of the excess electron spin e . Thus, the deterministic hybrid spatial-polarization CNOT gate on a two-photon system is completed.

Hybrid polarization-spatial CNOT gate on a two-photon system.

The schematic deterministic hybrid polarization-spatial CNOT gate on a two-photon system is shown in Figure 3(b). Here, the polarization state of photon a is the control qubit while the spatial state of photon b is the target qubit. The new circuit is derived from both subcircuits in Figure 2. First, the subcircuit S3 shown in Figure 2(b) is used to complete the controlled-phase-flip gate shown in equation (13) on the excess electron spin e and photon a , following the joint system $|\Phi_3\rangle_{ae}$ shown in equation (12). Then, using the subcircuit S2 shown in Figure 2(a) for the excess electron spin e and photon b , the total system is changed from $|\Phi_3\rangle_{ae}|\psi\rangle_b$ to

$$|\Phi_6\rangle_{abe} = \{|\uparrow\rangle_e[\alpha_1|R\rangle_a(\delta_1|b_1\rangle + \delta_2|b_2\rangle) + \alpha_2|L\rangle_a(\delta_2|b_1\rangle + \delta_1|b_2\rangle)] + |\downarrow\rangle_e[\alpha_1|R\rangle_a(\delta_1|b_1\rangle + \delta_2|b_2\rangle) - \alpha_2|L\rangle_a(\delta_2|b_1\rangle + \delta_1|b_2\rangle)]\} \otimes (\beta_1|R\rangle + \beta_2|L\rangle)_b \otimes (\gamma_1|a_1\rangle + \gamma_2|a_2\rangle). \quad (20)$$

Thus, after measuring the electron spin e under the orthogonal basis $\{|\uparrow\rangle, |\downarrow\rangle\}$, photons a and b may be changed into

$$|\Psi_4\rangle_{ab} = [\alpha_1|R\rangle_a(\delta_1|b_1\rangle + \delta_2|b_2\rangle) + \alpha_2|L\rangle_a(\delta_2|b_1\rangle + \delta_1|b_2\rangle)] \otimes (\beta_1|R\rangle + \beta_2|L\rangle)_b \otimes (\gamma_1|a_1\rangle + \gamma_2|a_2\rangle) \quad (21)$$

by performing the phase-flip operation R on the polarization of photon a for the measurement outcome $|\downarrow\rangle$ of the excess electron



spin e . So, the deterministic hybrid polarization-spatial CNOT gate on two photons is completed.

Hybrid spatial-polarization CNOT gate on a one-photon system.

The schematic deterministic hybrid spatial-polarization CNOT gate on a one-photon system is shown in Figure 3(c). Here, the spatial state of photon a is the control qubit while the polarization state of photon a is the target qubit. The circuit is similar to the one on a two-photon system, shown in Figure 3(a). The difference is that the two subcircuits S1 and S4 are implemented on only one photon. In detail, after passing the subcircuit S1 shown in Figure 2(a), the joint system of the electron spin e and photon a is $|\Phi_1\rangle_{ae}$, as shown in equation (6). Then, using the subcircuit S4 shown in Figure 2(b), the joint system $|\Phi_1\rangle_{ae}$ of the excess electron spin e and photon a is changed into

$$\begin{aligned} |\Phi_7\rangle_{ae} = & |\uparrow\rangle_e [\gamma_1 |a_1\rangle (\alpha_1 |R\rangle + \alpha_2 |L\rangle) \\ & + \gamma_2 |a_2\rangle (\alpha_2 |R\rangle + \alpha_1 |L\rangle)] \\ & + |\downarrow\rangle_e [\gamma_1 |a_1\rangle (\alpha_1 |R\rangle + \alpha_2 |L\rangle) \\ & - \gamma_2 |a_2\rangle (\alpha_2 |R\rangle + \alpha_1 |L\rangle)]. \end{aligned} \quad (22)$$

Thus, after measuring the excess electron spin e under the basis $\{|\uparrow\rangle, |\downarrow\rangle\}$, photon a may be changed into

$$\begin{aligned} |\Psi_5\rangle_a = & \gamma_1 |a_1\rangle (\alpha_1 |R\rangle + \alpha_2 |L\rangle) \\ & + \gamma_2 |a_2\rangle (\alpha_2 |R\rangle + \alpha_1 |L\rangle) \end{aligned} \quad (23)$$

by performing the phase-flip operation Z on the spatial modes of photon a for the measurement outcome $|\downarrow\rangle$ of the excess electron spin e . So, the deterministic hybrid spatial-polarization CNOT gate is completed on a one-photon system.

Hybrid polarization-spatial CNOT gate on a one-photon system.

The schematic deterministic hybrid polarization-spatial CNOT gate on a one-photon system is shown in Figure 3(d). Here, the polarization state of photon a is the control qubit while the spatial state of photon a is the target qubit. The circuit is similar to the one on a two-photon system, shown in Figure 3(b). The difference is that the two subcircuits S3 and S2 are implemented on only one photon. In detail, after passing the subcircuit S3 shown in Figure 2(b), the joint system of the electron spin e and photon a is $|\Phi_3\rangle_{ae}$ shown in equation (12). Then, using the subcircuit S2 shown in Figure 2(a), $|\Phi_3\rangle_{ae}$ is changed into

$$\begin{aligned} |\Phi_8\rangle_{ae} = & |\uparrow\rangle_e [\alpha_1 |R\rangle (\gamma_1 |a_1\rangle + \gamma_2 |a_2\rangle) \\ & + \alpha_2 |L\rangle (\gamma_2 |a_1\rangle + \gamma_1 |a_2\rangle)] \\ & + |\downarrow\rangle_e [\alpha_1 |R\rangle (\gamma_1 |a_1\rangle + \gamma_2 |a_2\rangle) \\ & + \alpha_2 |L\rangle (\gamma_2 |a_1\rangle + \gamma_1 |a_2\rangle)]. \end{aligned} \quad (24)$$

Thus, after measuring the electron spin e under the basis $\{|\uparrow\rangle, |\downarrow\rangle\}$, photon a may be changed into

$$\begin{aligned} |\Psi_6\rangle_a = & \alpha_1 |R\rangle (\gamma_1 |a_1\rangle + \gamma_2 |a_2\rangle) \\ & + \alpha_2 |L\rangle (\gamma_2 |a_1\rangle + \gamma_1 |a_2\rangle) \end{aligned} \quad (25)$$

by performing the phase-flip operation R on the polarization modes of photon a for the measurement outcome $|\downarrow\rangle$ of the excess electron spin e . So, the deterministic hybrid polarization-spatial CNOT gate is completed on one photon.

Discussion

Experimentally, the transition rules in equation (5) may fail due to decoherence and dephasing. The fidelities of our hyper-CNOT gates are reduced. The spin-dependent transition rule is imperfect and decreases the fidelities by a few percent if heavy-light hole mixing

is considered. Fortunately, the hole mixing can be reduced by improving the shape, size, and type of QDs³⁰. Although electron spin decoherence can also decrease the fidelities of the hyper-CNOT gates, however, this effect may be reduced by extending the electron coherence time to μs using spin echo techniques³⁰. The spin superposition states $|+\rangle$ and $|-\rangle$ are generated using nanosecond electron spin resonance microwave pulses or picosecond optical pulses⁴⁷, of which the preparation time (ps) is significantly shorter than the spin coherence time²⁸. Then, the Hadamard operation for transforming electron spin states $|\uparrow\rangle$ and $|\downarrow\rangle$ to $|+\rangle$ and $|-\rangle$ can be achieved.

In ideal conditions, one may neglect the cavity side leakage, and the reflection coefficients are $|r_0(\omega)| \approx 1$ and $|r_n(\omega)| \approx 1$. The corresponding fidelities of our six hyper-CNOT gates are nearly 100%. Unfortunately, it is impossible to neglect side leakage from the cavity in the experiment^{27-31,44-51}. The general fidelity is defined by $F = \langle \phi | \phi \rangle$, where $|\phi\rangle$ and $|\phi_f\rangle$ are the final states of an ideal condition and a real situation with side leakage, respectively. In the resonant condition with $\omega_c = \omega_e = \omega$, if the cavity side leakage is considered, the optical selection rules for a QD-cavity system given by the equation (4) become

$$\begin{aligned} |R\rangle|\uparrow\rangle & \mapsto r_0 |R\rangle|\uparrow\rangle, |R\rangle|\downarrow\rangle \mapsto r |R\rangle|\downarrow\rangle, |L\rangle|\uparrow\rangle \\ & \mapsto r |L\rangle|\uparrow\rangle, |L\rangle|\downarrow\rangle \mapsto r_0 |L\rangle|\downarrow\rangle. \end{aligned} \quad (26)$$

Due to the exchangeability of the polarization DOF and the spatial DOF of one photon with respect to random initial photon, the fidelities of the hybrid spatial-polarization CNOT and the hybrid polarization-spatial CNOT on a two-photon are same to these of the spatial-CNOT and the polarization CNOT on a two-photon, respectively. However, for the spatial-CNOT and the polarization CNOT, we cannot directly get the same fidelities from the exchangeability of polarization DOF and spatial DOF because the exchanging of two DOFs at one time may cause confusing implementation due to the different circuits of these hyper CNOT gates, shown in Figure 2. Moreover, from Figure 3 for the one-photon system, one cannot change the DOFs during the implementation process because the hyper-CNOT is not realized in a one-shot manner. Thus, we need to compute the fidelities of the spatial-CNOT and polarization-CNOT on a two-photon system and the hybrid spatial-polarization CNOT and the hybrid polarization-spatial CNOT on a one-photon system.

In detail, by replacing the optical selection rules in equation (5) with the ones in equation (26), using the same procedures as in the Results section, one can obtain the final states after the spatial CNOT gate on a two-photon system, polarization-CNOT gate on a two-photon system, hybrid spatial-polarization CNOT on a one-photon system, or hybrid spatial-polarization CNOT on a one-photon system. Therefore, the fidelities F of these four hyper-CNOT gates are

$$F_{SSD}^2 = \frac{(\delta_1^2 (\gamma_1^2 + 0.5\gamma_2^2 (r+r_0)) + \delta_2^2 (r\gamma_1^2 + 0.5r_0\gamma_2^2 (r+r_0)))^2}{\delta_1^2 (\gamma_1^2 + 0.5\gamma_2^2 (r^2 + r_0^2)) + \delta_2^2 (r^2\gamma_1^2 + 0.25\gamma_2^2 (r^2 + r_0^2)^2)}, \quad (27)$$

$$F_{SPD}^2 = \frac{(\beta_1^2 (\gamma_1^2 + 0.5\gamma_2^2 (r+r_0)) + \beta_2^2 (r\gamma_1^2 + 0.5r_0\gamma_2^2 (r+r_0)))^2}{\beta_1^2 (\gamma_1^2 + 0.5\gamma_2^2 (r^2 + r_0^2)) + \beta_2^2 (r^2\gamma_1^2 + 0.25\gamma_2^2 (r^2 + r_0^2)^2)}, \quad (28)$$

$$F_{SPS}^2 = \frac{(\gamma_1^2 (\alpha_1^2 + 0.5r\alpha_2^2) + 0.5\gamma_2^2 (r+r_0) (\alpha_1^2 + r_0\alpha_2^2))^2}{(\gamma_1^2 + 0.25\gamma_2^2 (r-r_0)^2) (\alpha_1^2 + r^2\alpha_2^2) + 0.25\gamma_2^2 (r+r_0)^2 (\alpha_1^2 + r_0^2\alpha_2^2)}, \quad (29)$$

$$F_{BSS}^2 = \frac{(\gamma_1^2 (\alpha_1^2 r + 0.5r_0 (r+r_0) \alpha_2^2) + \gamma_2^2 (\alpha_1^2 + 0.5(r+r_0) \alpha_2^2))^2}{\gamma_1^2 (r^2\alpha_1^2 + 0.25\alpha_2^2 (r^2 (r-r_0)^2 + r_0^2 (r+r_0)^2)) + \gamma_2^2 (\alpha_1^2 + 0.5\alpha_2^2 (r^2 + r_0^2))}, \quad (30)$$

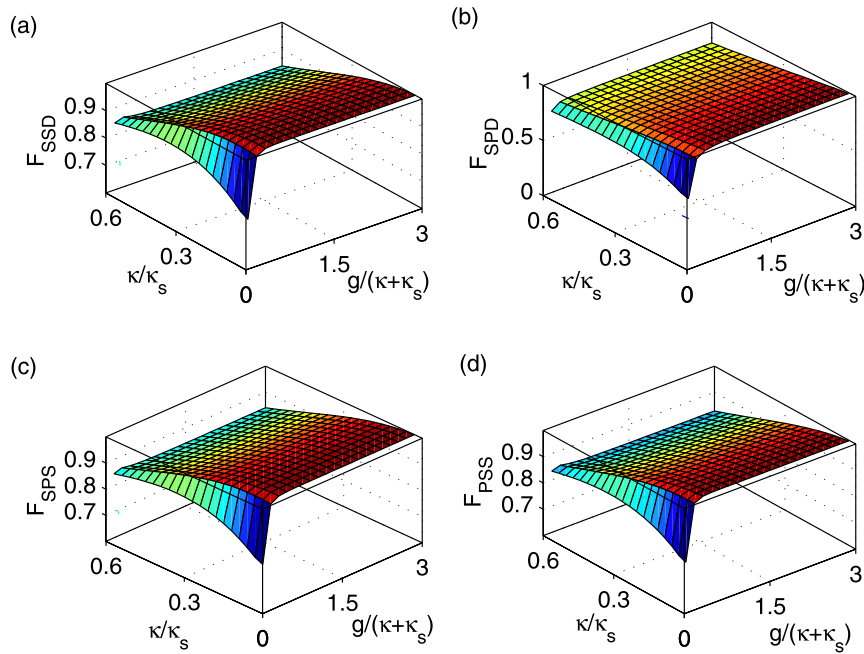


Figure 4 | Average fidelities of the present hyper-CNOT gates. (a) The average fidelity of the spatial-CNOT gate on a two-photon system. (b) The average fidelity of the polarization-CNOT gate on a two-photon system. (c) The average fidelity of the hybrid spatial-polarization CNOT gate on a one-photon system. (d) The average fidelity of the hybrid polarization-spatial CNOT gate on a one-photon system. The coupling strength is defined by $\varsigma = 0.1\kappa_s$. The average fidelity is computed as the expectation of random input photons.

where $\alpha_i, \beta_i, \gamma_i, \delta_i$ are the coefficients of the initial photons and satisfy $\alpha_1^2 + \alpha_2^2 = \beta_1^2 + \beta_2^2 = \gamma_1^2 + \gamma_2^2 = \delta_1^2 + \delta_2^2 = 1$, and $\alpha'_1 = \alpha_1 + \alpha_2$, $\alpha'_2 = \alpha_1 - \alpha_2$, $\beta'_1 = \beta_1 + \beta_2$, $\beta'_2 = \beta_1 - \beta_2$, $\gamma'_1 = \gamma_1 + \gamma_2$, $\gamma'_2 = \gamma_1 - \gamma_2$, $\delta'_1 = \delta_1 + \delta_2$, $\delta'_2 = \delta_1 - \delta_2$. We only consider the real r, r_0 and real coefficients $\alpha_i, \beta_i, \gamma_i, \delta_i$. Because these fidelities depend on the coefficients of the initial photons, we present them in Figure 4 as the expectations of the initial states by evaluating the average fidelity of 10^6 random initial photons. Here, $r_0 = \frac{\kappa' - 1}{\kappa' + 1}$ [from the equation (3)] and $r = \frac{(\kappa' - 1)/(1 + \kappa')^2 + 10g'^2}{1/(1 + \kappa')^2 + 10g'^2}$ [from the equation (2) and $\varsigma = 0.1\kappa_s$] under the resonant condition $\omega_c = \omega = \omega_e$ and $\kappa' = \kappa/\kappa_s$ and $g' = g/(\kappa_s + \kappa)$. Generally, strong coupling strength and the low side leakage and cavity loss rate (κ/κ_s) are all required for high fidelity. Experimentally, the strong coupling strength $g/(\kappa_s + \kappa)$ can be raised to 2.4 by improving the sample designs, growth, and fabrication^{48,49}. For our hyper-CNOT gates, if $g/(\kappa_s + \kappa) \approx 0.5$ and $\kappa/\kappa_s \approx 0$, their fidelities are greater than 90%. When the coupling strength $g/(\kappa_s + \kappa) \approx 2.4$ with $\kappa/\kappa_s \approx 0$, the fidelities are approximately 100%. If the side leakage and cavity loss rate are $\kappa/\kappa_s \approx 0.3$ for $g/(\kappa_s + \kappa) \approx 2.4$, the fidelities are greater than 95%. The side leakage and cavity loss rate have been reduced to $\kappa/\kappa_s \approx 0.7$ with $g/(\kappa_s + \kappa) \approx 1$ ^{30,43,44,50}. Recently, a quantum gate between the spin state of a single trapped atom and the polarization state of an optical photon contained in a faint laser pulse has been experimentally achieved⁵¹. We believe that their hybrid gate may soon be extended to our general hyper-CNOT gates on the two-photon system or the one-photon system because the main primitive gate of our CNOT gates is the controlled-phase-flip gate shown in equations (7) and (13).

In conclusion, we have investigated the possibility of parallel quantum computation based on two DOFs of photon systems, without using auxiliary spatial modes or polarization modes. We have constructed six deterministic hyper-controlled-not (hyper-CNOT) gates operating on the spatial-mode and the polarization DOFs of a two-photon system or a one-photon system. Compared with the hyper-CNOT gates on the same DOF of a two-photon system^{24,33–35},

our gates may be performed on different DOFs of two photons or one photon. Our schemes have also used fewer CPBS, which may be difficult in experiment. In contrast to the hybrid hyper-CNOT gates on the photon and stationary electron spins in quantum dots^{32,36}, our CNOT gates are ultimately realized on the photon system, and the excess electron spin is an auxiliary resource. Because the side leakage and cavity loss may be difficult to control or reduce for the electron-spin qubit and photonic qubits in the double-sided QD-cavity system, our gates are easier to implement experimentally than the hyper-parallel photonic quantum computation gates³⁷ using a double-sided QD-cavity system. Furthermore, their hyper-CNOT gates are only performed on a two-photon system, while our gates have also been implemented on a one-photon system. Even if the different DOFs may be easily changed, the operation of exchanging different DOFs is not convenient for a one-photon system because the hyper-CNOT is not realized in a one-shot manner. In detail, from the schematic circuits shown in Figure 3(c) and (d), one controlled-phase-flip gate is firstly performed on the auxiliary electron spin and one DOF, and then another controlled-phase-flip gate is performed on the auxiliary electron spin and the other DOF. Thus, one cannot exchange the DOFs after the controlled-phase-flip gate, and can only exchange the DOFs before the CNOT gate. This fact is important for the parallel quantum realization of large-scale quantum schemes such as the quantum Shor algorithm or the quantum search algorithm. Therefore, our results are distinct from all previous quantum logic gates on different photons^{32–37}. Our theoretical results show that two DOFs of photon systems can be used as independent qubits in quantum information processing. With these realizations, one half of the quantum resources may be saved. Of course, the hyper-CNOT gates may be affected by the cavity leakage, and spin coherence in quantum dots or the exciton coherence in experiment. With the recent experiments of QD-cavity system^{28–30} and the quantum gate between a flying optical photon and a single trapped atom⁵¹, our results are expected to be applicable for creating photon-photon entangled states from separable input states, large-scale quantum computation, or quantum communication.



Methods

Measurement of the excess electron spin e in QD. The excess electron spin e is measured using an auxiliary photon $|\psi\rangle_c = \frac{1}{\sqrt{2}}(|R\rangle + |L\rangle)_c|c_1\rangle$. Let the right-circular polarization $|R\rangle$ of photon c interact with the QD-cavity system [photon c passes a CPBS to splitter the circular polarizations $|R\rangle$ and $|L\rangle$, and then the $|R\rangle$ passes through the QD and combines with $|L\rangle$ of photon c using another CPBS]. Then, the final state of the complicated system becomes

$$\begin{aligned} \frac{1}{\sqrt{2}}(|R\rangle + |L\rangle)_c|c_1\rangle|\uparrow\rangle_e &\rightarrow -\frac{1}{\sqrt{2}}(|R\rangle - |L\rangle)_c|c_1\rangle|\uparrow\rangle_e, \\ \frac{1}{\sqrt{2}}(|R\rangle + |L\rangle)_c|c_1\rangle|\downarrow\rangle_e &\rightarrow \frac{1}{\sqrt{2}}(|R\rangle + |L\rangle)_c|c_1\rangle|\downarrow\rangle_e. \end{aligned} \quad (31)$$

Thus, the electron spin e can be determined by measuring the photon in the orthogonal basis $\left\{\frac{1}{\sqrt{2}}(|R\rangle \pm |L\rangle)\right\}$. The electron spin is $|\uparrow\rangle$ or $|\downarrow\rangle$ for the measurement outcome $\frac{1}{\sqrt{2}}(|R\rangle + |L\rangle)$ or $\frac{1}{\sqrt{2}}(|R\rangle - |L\rangle)$, respectively.

Single-sided QD-cavity system in quantum information processing based on two DOFs. The spatial-mode and the polarization DOFs may convert into each other if only one DOF is used for encoding information. There are many schemes on the polarization logic gates using the spatial-mode DOF as the assistant^{19,20,24,31–33}. Our hyper-CNOT gates show that the spatial-mode and the polarization DOFs of photonic states can be used independent qubits without auxiliary spatial modes. This is simpler than the one using double-side QD-cavity system³⁷. If two DOFs are independently used for encoding different information, their conversions may cause confusions for quantum information processing. For example, two DOFs of the photon system are used as the encoding qubit and the register qubit respectively, one cannot convert them during the Shor decomposition. Moreover, if the spatial-mode DOFs of some photon systems and the polarization DOFs of other photon systems are used as the same type of qubits in application, such as the register qubits in the Shor algorithm, great attentions should be paid because the circuits of six hyper-CNOT gates are different and cannot exchanged in experiment. Of course, the two DOFs of a photon may be used as a four-dimensional state, and the single-sided QD-cavity system can also be used to implement the quantum information process with this normalization of two DOFs.

- Nielsen, M. A & Chuang, I. L. (ed.) [Quantum Computation and Quantum Information] [216–271] (Cambridge University Press, Cambridge, 2000).
- Shor, P. W. Polynomial-time algorithms for prime factorization and discrete logarithms on a quantum computer. *SIAM J. Comput.* **26**, 1484–1509 (1997).
- Grover, L. K. Quantum mechanics helps in searching for a needle in a haystack. *Phys. Rev. Lett.* **79**, 325–328 (1997).
- Farhi, E. *et al.* A quantum adiabatic evolution algorithm applied to random instances of an NP-Complete problem. *Science* **292**, 472–475 (2001).
- Bennett, C. H. & Brassard, G. Quantum cryptography: Public key distribution and coin tossing. *Proc. IEEE Inter. Conf. Computers, Systems and Signal Process.*, Bangalore, India; DOI:10.1016/j.tmaid.2008.06.006 (1984).
- Bennett, C. H. *et al.* Teleporting an unknown quantum state via dual classical and Einstein-Podolsky-Rosen channels. *Phys. Rev. Lett.* **70**, 1895–1899 (1993).
- Barenco, A. & Ekert, A. K. Dense coding based on quantum entanglement. *J. Modern Opt.* **42**, 1253–1259 (1995).
- Barenco, A. *et al.* Elementary gates for quantum computation. *Phys. Rev. A* **52**, 3457–4467 (1995).
- Monroe, C., Meehof, D. M., King, B. E., Itano, W. M. & Wineland, D. J. Demonstration of a fundamental quantum logic gate. *Phys. Rev. Lett.* **75**, 4714–4717 (1995).
- Deutsch, D. Quantum computational networks. *Proc. R. Soc. Lond. A* **425**, 73–90 (1989).
- Schmidt-Kaler, F. *et al.* Realization of the Cirac-Zoller controlled-NOT quantum gate. *Nature* **422**, 408–411 (2003).
- Beenakker, C. W. J., DiVincenzo, D. P., Emary, C. & Kindermann, M. Charge detection enables free-electron quantum computation. *Phys. Rev. Lett.* **93**, 020501 (2004).
- Turchette, Q. A., Hood, C. J., Lange, W., Mabuchi, H. & Kimble, H. J. Measurement of conditional phase shifts for quantum logic. *Phys. Rev. Lett.* **75**, 4710–4713 (1995).
- Rauschenbeutel, A. *et al.* Coherent operation of a tunable quantum phase gate in cavity QED. *Phys. Rev. Lett.* **83**, 5166–5169 (1999).
- Gershenfeld, N. A. & Chuang, I. L. Bulk spin-resonance quantum computation. *Science* **275**, 350–356 (1997).
- Feng, G., Xu, G. & Long, G. Experimental realization of nonadiabatic Holonomic quantum computation. *Phys. Rev. Lett.* **110**, 190501 (2013).
- Li, X. *et al.* An all-optical quantum gate in a semiconductor quantum dot. *Science* **301**, 809–811 (2003).
- Knill, E., Laflamme, R. & Milburn, G. J. A scheme for efficient quantum computation with linear optics. *Nature* **409**, 46–52 (2001).

- Nemoto, K. & Munro, W. J. Nearly deterministic linear optical controlled-NOT gate. *Phys. Rev. Lett.* **93**, 250502 (2004).
- O'Brien, J. L., Pryde, G. J., White, A. G., Ralph, T. C. & Branning, D. Demonstration of an all-optical quantum controlled-NOT gate. *Nature* **426**, 264–267 (2003).
- Fleischhauer, M., Imamoglu, A. & Marangos, J. P. Electromagnetically induced transparency: optics in coherent media. *Rev. Mod. Phys.* **77**, 633–673 (2005).
- Schmidt, H. & Imamoglu, A. Giant Kerr nonlinearities obtained by electromagnetically induced transparency. *Opt. Lett.* **21**, 1936–1938 (1996).
- Hofmann, H. F., Kojima, K., Takeuchi, S. & Sasaki, K. Optimized phase switching using a single-atom nonlinearity. *J. Opt. B: Quantum Semiclass. Opt.* **5**, 218–221 (2003).
- Duan, L.-M. & Kimble, H. J. Scalable photonic quantum computation through cavity-assisted interactions. *Phys. Rev. Lett.* **92**, 127902 (2004).
- Menicucci, N. C., Flammia, S. T. & Pfister, O. One-way quantum computing in the optical frequency comb. *Phys. Rev. Lett.* **101**, 130501 (2008).
- Langford, N. K. *et al.* Efficient quantum computing using coherent photon conversion. *Nature* **478**, 360–363 (2011).
- Hu, C. Y., Young, A., O'Brien, J. L., Munro, W. J. & Rarity, J. G. Giant optical Faraday rotation induced by a single-electron spin in a quantum dot: applications to entangling remote spins via a single photon. *Phys. Rev. B* **78**, 085307 (2008).
- Hu, C. Y., Munro, W. J. & Rarity, J. G. Deterministic photon entangler using a charged quantum dot inside a microcavity. *Phys. Rev. B* **78**, 125318 (2008).
- Hu, C. Y., Munro, W. J., O'Brien, J. L. & Rarity, J. G. Proposed entanglement beam splitter using a quantum-dot spin in a double-sided optical microcavity. *Phys. Rev. B* **80**, 205326 (2009).
- Hu, C. Y. & Rarity, J. G. Loss-resistant state teleportation and entanglement swapping using a quantum-dot spin in an optical microcavity. *Phys. Rev. B* **83**, 115303 (2011).
- Bonato, C. *et al.* CNOT and Bell-state analysis in the weak-coupling cavity QED regime. *Phys. Rev. Lett.* **104**, 160503 (2010).
- Wei, H. R. & Deng, F. G. Universal quantum gates for hybrid systems assisted by quantum dots inside double-sided optical microcavities. *Phys. Rev. A* **87**, 022305 (2013).
- Wang, H. F., Zhu, A. D., Zhang, S. & Yeon, K. H. Deterministic CNOT gate and entanglement swapping for photonic qubits using a quantum-dot spin in a double-sided optical microcavity. *Phys. Lett. A* **377**, 2870–2876 (2013).
- Ren, B. C., Wei, H. R. & Deng, F. G. Deterministic photonic spatial-polarization hyper-controlled-not gate assisted by a quantum dot inside a one-side optical microcavity. *Laser Phys. Lett.* **10**, 095202 (2013).
- Wei, H. R. & Deng, F. G. Universal quantum gates on electron-spin qubits with quantum dots inside single-side optical microcavities. *Opt. Express* **22**, 593–607 (2014).
- Wang, T. J., Zhang, Y. & Wang, C. Universal hybrid hyper-controlled quantum gates assisted by quantum dots in optical double-sided microcavities. *Laser Phys. Lett.* **11**, 025203 (2014).
- Ren, B. C. & Deng, F. G. Hyper-parallel photonic quantum computation with coupled quantum dots. *Sci. Rep.* **4**, 4623 (2014).
- Ren, B. C., Wei, H. R., Hua, M., Li, T. & Deng, F. G. Complete hyperentangled-Bell-state analysis for photon systems assisted by quantum-dot spins in optical microcavities. *Opt. Express* **20**, 24664–24677 (2012).
- Wang, T. J., Lu, Y. & Long, G. L. Generation and complete analysis of the hyperentangled Bell state for photons assisted by quantum-dot spins in optical microcavities. *Phys. Rev. A* **86**, 042337 (2012).
- Young, A. B. *et al.* Quantum-dot-induced phase shift in a pillar microcavity. *Phys. Rev. A* **84**, 011803 (2011).
- Petta, J. R. *et al.* Coherent manipulation of coupled electron spins in semiconductor quantum dots. *Science* **309**, 2180 (2005).
- Brunner, D. *et al.* A coherent single-hole spin in a semiconductor. *Science* **325**, 70–72 (2009).
- Reithmaier, J. P. *et al.* Strong coupling in a single quantum dot-semiconductor microcavity system. *Nature* **432**, 197–200 (2004).
- Yoshie, T. *et al.* Vacuum Rabi splitting with a single quantum dot in a photonic crystal nanocavity. *Nature* **432**, 200–203 (2004).
- Warburton, R. J. *et al.* Charged excitons in self-assembled semiconductor quantum dots. *Phys. Rev. Lett.* **79**, 5282 (1997).
- Hu, C. Y. *et al.* Optically detected magnetic resonance of excess electrons in type-I quantum wells with a low-density electron gas. *Phys. Rev. B* **58**, R1766–R1769 (1998).
- Press, D., Ladd, T. D., Zhang, B. & Yamamoto, Y. Complete quantum control of a single quantum dot spin using ultrafast optical pulses. *Nature* **456**, 218–221 (2008).
- Loo, V. *et al.* Quantum dot-cavity strong-coupling regime measured through coherent reflection spectroscopy in a very high-Q micropillar. *Appl. Phys. Lett.* **97**, 241110 (2010).
- Yoshie, T. *et al.* Vacuum Rabi splitting with a single quantum dot in a photonic crystal nanocavity. *Nature* **432**, 200–203 (2004).
- Reitzenstein, S. *et al.* AlAs/GaAs micropillar cavities with quality factors exceeding 150,000. *Appl. Phys. Lett.* **90**, 251109 (2007).



51. Reiserer, A., Kalb, N., Rempe, G. & Ritter, S. A quantum gate between a flying optical photon and a single trapped atom. *Nature* **508**, 237–240 (2014).

Acknowledgments

This work is supported by the National Natural Science Foundation of China (Nos.61303039), Open Foundation of State key Laboratory of Networking and Switching Technology (Beijing University of Posts and Telecommunications) (No.SKLNST-2013-1-11), Fundamental Research Funds for the Central Universities (No.2682014CX095), and Science Foundation Ireland (SFI) under the International Strategic Cooperation Award Grant Number SFI/13/ISCA/2845.

Author contributions

L.M.X. proposed the theoretical method and wrote the main manuscript text. L.M.X. and W.X. reviewed the manuscript.

Additional information

Competing financial interests: The authors declare no competing financial interests.

How to cite this article: Luo, M.-X. & Wang, X. Parallel Photonic Quantum Computation Assisted by Quantum Dots in One-Side Optical Microcavities. *Sci. Rep.* **4**, 5732; DOI:10.1038/srep05732 (2014).



This work is licensed under a Creative Commons Attribution-NonCommercial-NoDerivs 4.0 International License. The images or other third party material in this article are included in the article's Creative Commons license, unless indicated otherwise in the credit line; if the material is not included under the Creative Commons license, users will need to obtain permission from the license holder in order to reproduce the material. To view a copy of this license, visit <http://creativecommons.org/licenses/by-nc-nd/4.0/>